

Uncoiling transition for DNA in solution

Carlos E. Galindo* and J. B. Sokoloff

Physics Department, Northeastern University, Boston, Massachusetts 02115

(Received 7 August 1995)

We study a simple DNA helix model, consisting of two infinite chains of evenly spaced charges to represent the phosphate groups, wound in a helix which lies on an imaginary cylindrical surface. The change in the free energy per helix charge between coiled and uncoiled conformations of the helix in solution is studied as a function of the charge per unit length along the helix axis. This allows us to study the effects of the solution on the helix stability and coiling. The change in the free energy is calculated from Soumpasis's pair potential of mean force, applied to all pairs of helix charges [D. M. Soumpasis, Proc. Natl. Acad. Sci. U.S.A. **81**, 5116 (1984)]. The local counterion concentration is calculated from the counterion radial distribution that results from solving the Poisson-Boltzmann equation for an infinite uniformly charged cylinder [R. M. Fuoss, A. Katchalsky, and S. Lifson, Proc. Natl. Acad. Sci. **37**, 579 (1951)], whose linear charge density is equal to the charge per unit length along the helix axis. Our results show that the helix is less stable on decreasing bulk dielectric constant and more stable on increasing counterion radius. Experimental data are discussed on DNA in solutions with water, ethanol, and methanol as the solvent.

PACS number(s): 87.15.-v

I. INTRODUCTION

In aqueous solution at neutral pH and room temperature, deoxyribonucleic acid (DNA) [1] is a polyion, whose total charge is compensated by small mobile *counterions*. In a simple way, a DNA strand can be thought of as a macromolecular chain formed from nucleotides. A nucleotide is formed from a sugar (furanose) ring to which a planar molecule, or base (A , G , T , or C), and a charged phosphate group are attached. In our paper, we assume that the only charges on the DNA polyion are at the centers of the phosphate groups.

DNA helices show structural variety [1–3], which depends on environmental factors, such as counterion, solvent, and temperature, as well as retained salt and relative humidity in crystallographic samples. An ideal infinite helix is left invariant under a combination of a *translation* along the helix axis and a *rotation* about the helix axis, which is the space group of the helix. From measurements on right-handed double helices, it is well known that axial translations and rotations per nucleotide range from 2.56 to 3.41 Å and from 45° to 30°, respectively.

The phosphate group positions are important in our calculations. Soumpasis [4] and his group [5] have developed a method to calculate the effects of the solution on the relative stability between two polyion conformations, and their results have been confirmed experimentally. In Soumpasis's method, which is used in our paper and reviewed in Sec. II, the change in the free energy between two polyion conformations is calculated using statistically averaged interactions, or potentials of mean force (PMF's). Interactions between charged phosphate groups in the solution are calculated from the pair PMF, which includes the effects of

the salt, such as charge screening and hard-core correlations due to the finite size of the ions. In the treatment of Refs. [4] and [5], the solution is allowed to flow freely into the interior of the DNA molecule (i.e., into the region enclosed by the double helix of phosphate group charges). In contrast, in our treatment, we do not allow the solution to penetrate into this region.

A DNA double helix can be treated as a straight cylinder over a distance of many base pairs, because of steric constraints and electrostatic forces of short range (base stacking interactions), which act perpendicularly to the base planes [1]. On the basis of crystallographic atomic coordinates [6–8] of various DNA right-handed helices, which display different axial translations and rotations per nucleotide, the radial distance of the phosphate groups to the axis is not seen to vary substantially. Section III presents a double helix model, formed from two chains of charges, in which the axial translation and rotation per helix charge vary to describe coiling or winding, while the radial distance from a charge to the axis and the distance between two consecutive charges on the same chain are kept fixed during the process of coiling.

Our investigation was motivated by a desire to understand the dissociation of a double stranded DNA into single strands. It is experimentally known that a DNA double helix in aqueous solution is unstable at very low salt concentrations [9–12], i.e., natural DNA in a concentration of less than $10^{-4}M$ at room temperature [12]. Moreover, at moderate concentrations ($\sim 0.1M$), DNA is unstable at high temperatures ($\sim 85^\circ C$). As recognized, the process of dissociation of the two strands, called denaturation, involves two steps [1,13]: the uncoiling of the helix and the separation of the strands in which a complete breaking of the hydrogen bonds takes place. In our paper, we only treat the coiling-uncoiling of the double helix (the secondary structure) and the associated change in the free energy.

We describe the DNA double helix and the solution as two interdependent systems. The solution, determined by the

*Present address: Departamento Academico de Computacion, Instituto Tecnologico Autonomo de Mexico, Rio Hondo No. 1, Col. Tizapan, San Angel, DF, CP 04930, Mexico.

solvent, concentration, and type of counterion, has been considered to play an important role in DNA stability and conformation [1,9]. At high dilution, the molecule unwinds and elongates [14] before the separation of the strands takes place. Experiments have shown that the temperature of dissociation increases with increasing salt concentration [1] and this stabilizing factor of salt was attributed to the screening of the electrostatic repulsion between charged groups on either strand [15,16].

The theory of polyelectrolytes (charged polyions in solution) [17,18] is found in early theoretical studies of DNA denaturation [15,16,19]. In these studies, effects of the ionic concentration on the DNA melting temperature, the counterion distribution, and the counterion binding, were addressed by solving the Poisson-Boltzmann (PB) equation. During the last two decades, there has been a substantial development in the statistical theory of ionic solutions, and because of this development highly concentrated ionic solutions ($>2M$) can be more satisfactorily described [4,20].

In our treatment, the double helix charges are positioned on an imaginary cylindrical surface for reasons that were discussed earlier. The counterion distribution is calculated as if the charge on the double helix were uniformly distributed on a cylinder. In the early 1950s, an analytical integration of the PB equation for a uniformly charged infinite cylinder model was introduced [21,22] (the charge in solution is only due to the counterions in these treatments). As shown in these early studies, the cylinder *linear charge density* is an important parameter for determining the counterion distribution. In Sec. IV, to determine the local concentration of counterions at the cylinder surface, the counterion distribution around a charged cylinder is calculated from the PB equation of Ref. [21]. The linear charge density of the cylinder is equal to the charge per unit length along the axis of the double helix, which depends on the extent of coiling. Use of the PB equation is supported as a first approximation by Monte Carlo simulations on the ionic distribution surrounding a uniformly charged cylinder [23] without co-ions (ions with a charge of the same sign as the DNA polyion) and with counterions of small radii, compared to the DNA radius. In addition, there are Monte Carlo simulations using a more detailed molecular structure of the DNA polyion, based on experimental coordinates [24], which investigate the dielectric saturation of water near DNA. The radial counterion distribution that results from these simulations shows that the PB equation, which underestimates the counterion concentration near the DNA polyion by 18%, is qualitatively correct. We use the PB equation as a first approximation to determine the counterion concentration near the DNA polyion, which is best treated by introducing a dielectric constant smaller than the bulk value for the solvent close to the polyion. The available information on the value of the dielectric constant for the solvent at close distances is unclear [24]; however, our calculations involve other parameters that are well determined by experiments.

Manning elaborated on the notion of counterion binding in his theory of counterion condensation, which in its original form [25,26] is based on modeling a polyion as a uniform distribution of charge on a line of infinite length in a dilute salt solution. According to Manning, the counterions, treated as point charges, will condense on a polyion with a linear

charge density higher than a critical value; consequently, the polyion is partially neutralized. Studies that describe counterion condensation based on the PB equation for a charged cylinder have been published as well [27–29]. In contrast to the treatment given in Refs. [26] and [27], our treatment models the DNA molecule as a double helix of charge. We calculate the free energy difference between this double helix and the same charges with the double helix unwound, using the approximate treatment inherent in the potential of mean force (mainly the Kirkwood approximation). More recently, it was found that condensation of counterions is increased if the dielectric constant for the solvent near the DNA polyion is lower than the bulk value [24,30]. Furthermore, this is consistent with measurements on highly concentrated ionic solutions [31–33] showing that the dielectric constant is lower than the value of the pure solvent. Because of the above, in solving the PB equation in Sec. IV, we have assumed the dielectric constant has two values, one at large distances from the cylinder equal to the value for a bulk solvent and a smaller value close to the cylinder surface.

In Sec. II we describe Soumpasis's method to calculate the effects of the solution on the change in the free energy between two polyion conformations. In Sec. III, the helix model polyion and its parameters are introduced. In Sec. IV, to determine the local concentration at the cylinder surface we calculate the counterion distribution by the PB equation for an infinite uniformly charged cylinder. Section V is a discussion of the results.

II. THE POTENTIAL OF MEAN FORCE

We summarize some important points about Soumpasis's method [4] to calculate the effects of the solution on a polyion conformation, which is given by the positions of the charges on the polyion (for DNA, the positions of the phosphate groups). In the absence of counterion binding, the solution ions are considered to form a diffuse cloud. The solvent, considered as a continuous medium, is modeled by a dielectric constant. As in the Debye-Hückel (DH) theory of electrolytes, the solution degrees of freedom (ionic cloud and solvent) are considered statistically averaged, while the coordinates of the polyion charges remain as parameters of the free energy [34], or the potential of mean force. By this procedure, fast and slow processes are distinguished. Soumpasis [4] and his group [5] calculated the change in the free energy between two DNA conformations in solution, using approximations to the PMF, suggested by statistical mechanical theories [4,20].

For a given polyion conformation X determined by the positions of the polyion charges, two contributions to the free energy $F(X)$ are distinguished;

$$F(X) = F_0(X) + F_1(X), \quad (2.1)$$

where $F_1(X)$ includes the statistically averaged interactions of the polyion charges in the solution, and $F_0(X)$ includes all other interactions, such as hydrophobic interactions, DNA chemical bonds, dispersion forces, and base stacking, which are assumed to be independent of the solution up to a first approximation. For a second conformation Y , there is a similar form for the free energy:

$$F(Y) = F_0(Y) + F_1(Y). \quad (2.2)$$

As assumed, $F_0(Y)$ is not significantly different from $F_0(X)$ after changes in the solution, such as a change in the counterion distribution; hence, the change in the free energy between conformation X and conformation Y can be obtained by subtracting Eq. (2.1) from Eq. (2.2), giving

$$\Delta F(Y, X) \equiv F(Y) - F(X) = F_1(Y) - F_1(X). \quad (2.3)$$

A further approximation is introduced in calculating $F_1(X)$ and $F_1(Y)$ by adding all *pair* interactions between charged phosphate groups. The pair PMF is used to calculate interactions between pairs of phosphate groups. In Soumpasis's study [4], the ionic solution is formed by the polyion phosphate groups, which are treated as ions, and the surrounding ions (or counterions).

An ionic solution can be thought of as a gas of charged hard spheres in a continuous medium, the solvent. In the simplest case, the solution is formed by ions of two kinds, q_1 and q_2 , where $q_1 = -|e|$ and $q_2 = |e|$ ($|e| = 4.8032 \times 10^{-10}$ esu). Let n_1 and n_2 denote the number of ions per unit volume for each kind of ion. The free energy of two q_1 ions, considered fixed at a distance r , is the pair PMF used in the calculation; all other ions and the solvent are statistically averaged. At low concentrations, the PMF is a DH screened Coulomb interaction. At high concentrations, hard-sphere (HS) correlations become important. In our calculations we use an analytical expression of the pair PMF suggested by Olivares and McQuarrie [20] and used by Soumpasis [4], which shows these features:

$$w(r) = w^{\text{HS}}(r; \{n_i\}, \sigma, T) + w^{\text{DH}}(r; \{q_i\}, \{n_i\}, \sigma, T), \quad (2.4a)$$

where $\{q_i\}$ and $\{n_i\}$ denote the charges and the number of ions per unit volume, for each ion type i , respectively [for simplicity, r is assumed to be the only explicit parameter in $w(r)$]. In the last equation, the first term is

$$w^{\text{HS}}(r; \{n_i\}, \sigma, T) = -k_B T \ln g(r; \{n_i\}, \sigma), \quad (2.4b)$$

where $g(r; \{n_i\}, \sigma)$ is the pair correlation function of a hard-core potential, which depends on the concentration of hard spheres and the minimum distance of approach, σ (between a charge q_1 and a counterion q_2). The second term is

$$w^{\text{DH}}(r; \{q_i\}, \{n_i\}, \sigma, T) = \frac{q_1^2}{\bar{\epsilon}(1+k\sigma)} \frac{\exp[-k(r-\sigma)]}{r}, \quad (2.4c)$$

where $\bar{\epsilon}$ is the dielectric constant for the solvent and

$$k = \left(\frac{4\pi \sum_i n_i q_i^2}{\bar{\epsilon} k_B T} \right)^{1/2} \quad (2.4d)$$

is the inverse DH screening length, which characterizes the range of the electrostatic interaction.

Throop and Bearman [35] have evaluated the solution to the Percus-Yevick equation numerically and tabulated the radial distribution function for the hard-sphere potential. The

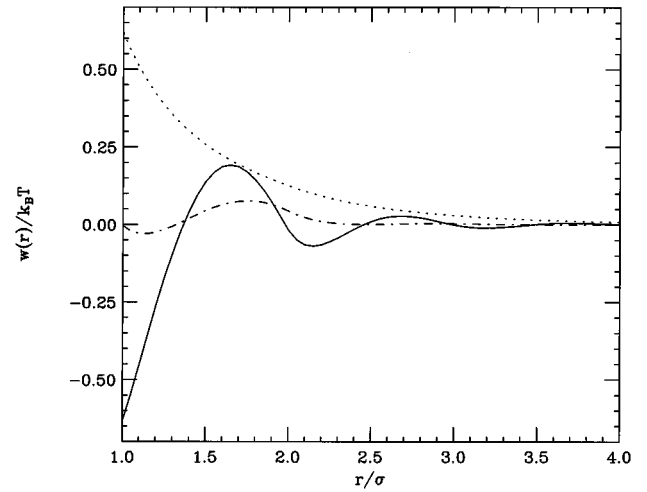


FIG. 1. The potential of mean force (PMF), from Eq. (2.4a), of two unit charge ions of equal sign in an ionic solution. Ions of two types form the solution, $q_1 = -|e|$ and $q_2 = |e|$, where $|e| = 4.8032 \times 10^{-10}$ esu. Ions of each type are in equal concentrations, $n_1 = n_2$ (the number of hard spheres per unit volume is $2n_1$). The molar salt concentration (M), c_1 from Eq. (2.5), for the examples is $0.4M$ (dotted line), $2.0M$ (dot-dashed line), and $4.0M$ (solid line). At high concentrations, there is a high Coulomb screening, and hard-core correlations are important, which is shown by the nonmonotonic solid line. Other parameters are $\bar{\epsilon} = 78.85$, $T = 25^\circ\text{C}$, and $\sigma = 5 \text{ \AA}$.

analytical expression for this function is given in Refs. [35] and [36]. A computer program, provided in Appendix D of Ref. [37], evaluates the Percus-Yevick correlation function with a modification [38] in agreement with Monte Carlo data for hard spheres. The PMF obtained from Eq. (2.4a), using in Eq. (2.4b) the Percus-Yevick correlation function, is displayed in Fig. 1; the energy of interaction of two charges, q_1 , is plotted as a function of the separation r . In the example, we have considered a case where $q_1 = -|e|$, $q_2 = |e|$, and $n_1 = n_2$; the molar salt concentration (M) is calculated from

$$c_1 = \frac{n_1}{6.022 \times 10^{-4}}, \quad (2.5)$$

where $2n_1$ is the number of hard spheres per \AA^3 . If the salt concentration is high enough, the Coulomb repulsion is screened, and Eq. (2.4b) becomes important, showing the effects of the ion hard core.

III. HELIX AND UNCOILING TRANSITION

In Table I we show a list of conformation parameters of various types of DNA. The x-ray crystallographic data on the phosphate group atomic coordinates were obtained from several references [6–8]. The right-handed helix model that is presented in this section is based on these measurements.

The double helix model is made from two interwound infinite linear chains of evenly spaced unit charges, due to the phosphate groups, on an imaginary cylindrical surface with a radius denoted by a'_0 . Even though the four cases presented in Table I correspond to various conditions of rela-

TABLE I. DNA double helix parameters which are obtained from experimental measurements. References are listed in this table. The definitions of the parameters are given in Sec. III of text.

DNA	a'_0 (Å)	\bar{d}_{pp} (Å)	$\bar{\psi}_0$ (deg)	\bar{h}_0 (Å)	d_{pp} (Å)	ψ_Y (deg)	$h(\psi_Y)$ (Å)	Ref.
A	8.92	18.549	138.4	8.12	5.637	32.7	2.56	[6]
B	8.91	18.228	169.6	4.16	6.461	36.0	3.38	[6]
C	9.05	16.903	137.8	0.74	6.842	38.6	3.32	[7]
D	7.86	16.227	176.8	4.05	6.736	45.0	3.03	[8]

tive humidity, retained salt, and counterion type, the radius a'_0 is not substantially changed in A-DNA, B-DNA, and C-DNA. In D-DNA, which is considerably coiled compared to B-DNA and C-DNA, a'_0 changes by about 1 Å. Since our assumption that a'_0 does not vary significantly among several different forms of DNA does not hold for Z-DNA, our method is not valid for treating it.

The distance between two consecutive charges on the same chain is denoted by d_{pp} and it is measured from one charge to the other in a straight line. As mentioned in the Introduction, the sugar ring conformation determines the distance between consecutive phosphate groups in a DNA strand backbone; this distance corresponds to d_{pp} . The difference in d_{pp} between the A-genus DNA and the B-genus DNA is about 1 Å (A-DNA belongs to the A genus; B-DNA, C-DNA, and D-DNA belong to the B genus).

For clarity, the z axis of a cylindrical system of coordinates is used as the axis of the helix. Double stranded DNA can be thought of as formed by repeating the nucleotide pair, bound by two complementary bases. The positions of a pair of charges associated with a nucleotide pair can be used to generate the positions of the consecutive pairs of charges by a rotation about the axis, ψ_Y , and a translation along the axis, $h(\psi_Y)$. The double helix is constructed by repeated application of the combined translation and rotation upon the coordinates of the first pair of charges. The translation along the z axis is

$$h(\psi_Y) = \sqrt{(d_{pp})^2 - (2a'_0 \sin[\psi_Y/2])^2} \quad \text{for } 0 \leq \psi_Y < 180^\circ, \quad (3.1)$$

where the angle of rotation ψ_Y is measured on a plane perpendicular to the axis, as an azimuthal angle, and $(d_{pp})^2 - (2a'_0 \sin[\psi_Y/2])^2 \geq 0$.

The distance between a pair of charges that correspond to the phosphate groups in a pair of complementary nucleotides is denoted by \bar{d}_{pp} , measured from one charge to the other in a straight line. In the B-DNA conformation [1] the base pair lies nearly in a plane, with one phosphate group above and the other below the base pair plane. As seen in Table I, the distances \bar{d}_{pp} of the four types of DNA are close in value, within approximately 2 Å. This distance is possibly due to the hydrogen bonding, which has a certain equilibrium length, the base pair, and the stacking interactions that restrict the base pair to be nearly on a plane (this plane is not necessarily perpendicular to the axis). The change in the azimuthal angle between the two charge positions of this pair of charges is denoted by $\bar{\psi}_0$. In this section, the quantities that depend on the relative position between the two helices are

denoted with a bar over them. The projection along the z axis of the distance between the pair of charges is

$$h^-_0 = \sqrt{(\bar{d}_{pp})^2 - (2a'_0 \sin[\bar{\psi}_0/2])^2} \quad \text{for } 0 < \bar{\psi}_0 \leq 180^\circ, \quad (3.2)$$

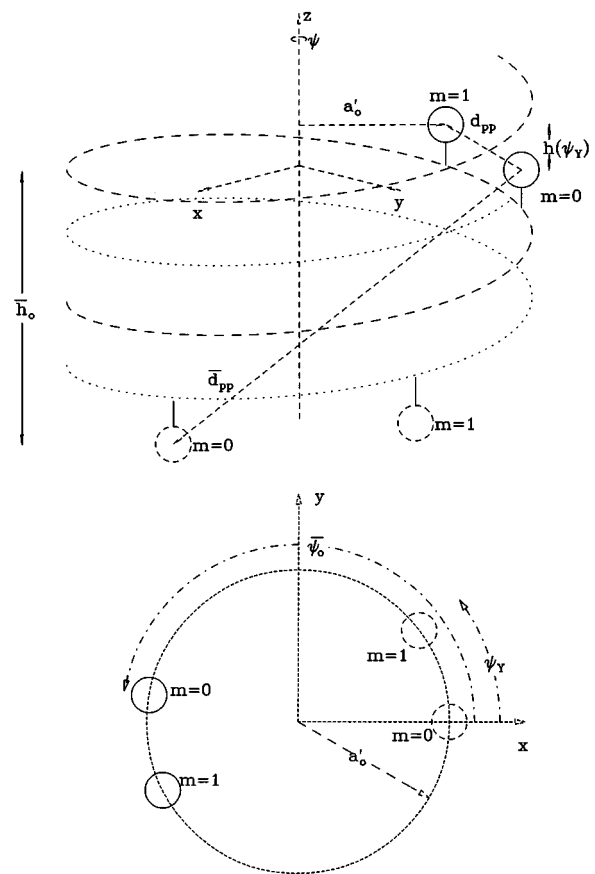


FIG. 2. (a) Two infinite chains of charges in a right-handed double helix wound on an axis along the z direction. Each pair of charges, which correspond to the phosphate groups on two complementary nucleotides, is numbered by a consecutive integer m . Charges on one chain are shown by solid lines, and charges on the other chain are shown by dashed lines; only the charges in the pairs $m=0$ and $m=1$ are displayed. The length parameters a'_0 , \bar{h}_0 , d_{pp} , and \bar{d}_{pp} and $h(\psi_Y)$, described in Sec. III of the text, are shown. (b) Projection on the x - y plane of the charges shown in (a). Each pair of charges, which correspond to the phosphate groups on two complementary nucleotides, is numbered by a consecutive integer m . Charges on one chain are depicted in solid lines, and charges on the other chain are in dashed lines; only four charges (the pairs, $m=0$ and $m=1$) are displayed. The helix axis is along the z direction. The angles $\bar{\psi}_0$ and ψ_Y , described in Sec. III of the text, are shown.

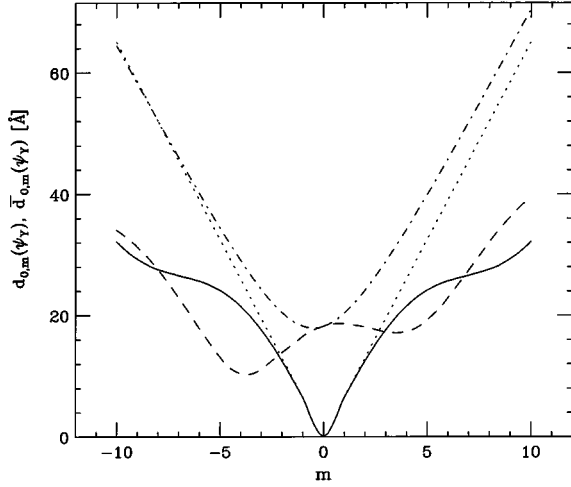


FIG. 3. The distances from a reference charge (in the pair denoted by $m=0$) to the other charges in the double helix model. The values of the parameters for the helix are taken from the B model of Table II. The coiled and uncoiled conformations are shown. For the coiled helix, $\psi_Y=36.6^\circ$ is assumed; for the uncoiled helix, $\psi_Y=0$. For $d_{0,m}(\psi_Y)$ of Eq. (3.3), the solid line and dotted line represent coiled and uncoiled conformations, respectively. For $\bar{d}_{0,m}(\psi_Y)$ of Eq. (3.4), the dashed line and dot-dashed line represent coiled and uncoiled conformations, respectively. The lines are drawn to highlight the points calculated from the above equations. It is seen that the curves for the charges on the same chain as the reference charge are symmetrical with respect to a plane crossing $m=0$ (solid and dotted lines).

where $(\bar{d}_{pp})^2 - (2a'_0 \sin[\bar{\psi}_0/2])^2 \geq 0$ and $\bar{\psi}_0$ is chosen within $0 < \bar{\psi}_0 \leq 180^\circ$. (The formula is not changed if instead of $\bar{\psi}_0$ the complementary angle $360^\circ - \bar{\psi}_0$ is used.)

In Figs. 2(a) and 2(b), the helix model is illustrated, with only two pairs of charges shown for simplicity. For clarity and notation, an integer m is assigned to each pair of charges associated with a complementary nucleotide pair, considering each pair of charges labeled in this way as one unit. We choose m to increase along the positive z axis and two consecutive integers are associated with two consecutive pairs of charges.

From given values of the parameters a'_0 , d_{pp} , $\bar{\psi}_0$, and \bar{d}_{pp} , and the angle ψ_Y , the positions of all helix charges can be determined with respect to a charge, used as a reference point, in the pair of charges designated by $m=0$. Distances from charges on the same chain as the reference charge are

$$d_{0,m}(\psi_Y) = \sqrt{[mh(\psi_Y)]^2 + [2a'_0 \sin(m\psi_Y/2)]^2}. \quad (3.3)$$

Distances from charges on the opposite chain to the reference charge are

$$\bar{d}_{0,m}(\psi_Y) = \sqrt{[mh(\psi_Y) - \bar{h}_0]^2 + \{2a'_0 \sin[(m\psi_Y - \bar{\psi}_0)/2]\}^2}, \quad (3.4)$$

where $m = \pm 1, \pm 2, \pm 3, \dots$, and $h(\psi_Y)$, and h_0 are given in Eqs. (3.1) and (3.2), respectively. For consistency of Eqs. (3.1) and (3.3), $d_{0,1}(\psi_Y) \equiv d_{pp}$; also of Eqs. (3.2) and (3.4), $\bar{d}_{0,0}(\psi_Y) \equiv \bar{d}_{pp}$. Figure 3 highlights the distances from the

reference charge, in the pair $m=0$, to near charges from above and below, calculated from Eqs. (3.3) and (3.4). (Coiled and uncoiled conformations for the double helix are presented. The uncoiled conformation represents the charges along two parallel lines.)

The following points are made to complete the discussion on Table I. B -DNA samples are generally obtained at approximately 92% of relative humidity with Na^+ as the counterion. A -DNA, C -DNA, and D -DNA samples are obtained at approximately 75% of relative humidity or even less. C -DNA is generally prepared in Li^+ salt, as seen in Table 9.1 of Ref. [1]. D -DNA is obtained under the minimum bulk salt concentration [8] which would normally give the A -DNA; however, the ionic concentration near a D -DNA molecule is not necessarily small enough to compensate for the higher charge per unit length, which is proportional to $1/h(\psi_Y)$. Reference [39] is an interesting early study on the atomic coordinates of DNA.

To describe coiling-uncoiling of the helix, we consider two conformations: the first, X , in which the helix is completely uncoiled, $\psi_Y=0$, and $h(0)=d_{pp}$ (i.e., two chains of charges parallel at a distance $2a'_0 \sin[\psi_0/2]$); the second conformation, Y , in which the helix is coiled with an angle ψ_Y , and $h(\psi_Y) < d_{pp}$, from Eq. (3.1). In considering the two conformations, the parameters a'_0 , d_{pp} , \bar{d}_{pp} , and $\bar{\psi}_0$, are kept constant. The charge per unit length along the axis of the double helix, which is proportional to $1/h(\psi_Y)$, is an important parameter for determining the concentration of counterions near the polyanion, using the PMF of Eq. (2.4a) of Sec. II. The concentration of counterions near the polyanion is calculated in Sec. IV.

In the final paragraphs, we give the formula for the change in the free energy between the two conformations; this discussion is based on the discussion presented in Sec. II. The change in the free energy between the two conformations, $\Delta F(Y,X)$ in Eq. (2.3), is calculated from the statistically averaged interactions of *all* phosphate groups in solution. The change in the free energy *per helix charge*, $\Delta W(Y,X)$, can be obtained by adding all pair interactions between *one* charge and all other charges on the double helix. To calculate the pair interactions we use the PMF $w(r)$ defined in Eq. (2.4a). The distances between a particular charge and all other charges on the same strand, $d_{0,m}(\psi_Y)$, or on the opposite strand, $\bar{d}_{0,m}(\psi_Y)$, are obtained from Eqs. (3.3) and (3.4), respectively. Therefore the change in free energy per helix charge between the two conformations is

$$\Delta W(Y,X) \equiv \sum_{m=-\infty}^{m=\infty} \delta W_m, \quad (3.5a)$$

where

$$\delta W_m = W_m(Y) - W_m(X), \quad (3.5b)$$

and

$$W_m(Y) = \{w[d_{0,m}(\psi_Y)] + w[\bar{d}_{0,m}(\psi_Y)]\}_{\psi_Y \neq 0}, \quad (3.5c)$$

$$W_m(X) = \{w[d_{0,m}(\psi_Y)] + w[\bar{d}_{0,m}(\psi_Y)]\}_{\psi_Y = 0}, \quad (3.5d)$$

where the integer m labels the charge pairs corresponding to complementary nucleotides.

In Sec. IV we calculate the counterion distribution around the double helix by solving the PB equation of a uniformly charged infinite cylinder. Once the counterion distribution is obtained, the salt concentration n at the cylinder surface can be obtained. This calculation is shown in Eq. (4.13) of the following section. The charge per unit length along the double helix axis is calculated from

$$\lambda = \frac{2q'}{h(\psi_Y)}, \quad (3.6)$$

where $h(\psi_Y)$ is given by Eq. (3.1) and q' is a charge on the double helix, the phosphate group charge.

The equilibrium conformation of the helix is found by minimizing the change in the free energy, Eq. (3.5a), as a function of the charge per unit length along the axis given in Eq. (3.6).

IV. DISTRIBUTION OF COUNTERIONS IN SOLUTION

In Sec. III, the helix charges were positioned on an imaginary cylindrical surface of radius a'_0 . In this section, the counterion distribution around the double helix is calculated as if the double helix were a uniformly charged cylinder of infinite length. The linear charge density of the cylinder is determined by Eq. (3.6). The calculations are based on solving the Poisson-Boltzmann equation for an impenetrable uniformly charged cylinder of radius a_0 , in which $a_0 = a'_0 + \sigma$, where σ is the minimum distance of approach of a counterion to the center of a charge on the polyion. Results in this section are based on an analytical solution of the PB equation [21] of an infinite charged cylinder with counterions.

Studies of DNA based on an infinite rigid cylinder model can be found [19]. This model assumes that the cylinder is the equilibrium conformation, ignoring the fluctuations around this conformation and bending. In addition, the infinite model might not be appropriate to describe DNA in solution; for example, when the solution is very dilute (i.e., the screening length is larger than the characteristic length scales associated with a DNA molecule, e.g., the radius of the molecule, the total length, or the radius of curvature). The cylinder represents a negatively charged polyion, on account of the phosphate group charges. The counterions are assumed to form a diffuse cloud.

The PB equation significantly simplifies the equilibrium analysis of the small ions in solution. The continuous model has been chosen to simplify the calculations; however, it is only appropriate as long as the discrete nature of the charges can be neglected. The use of the PB equation as a first approximation is supported by Monte Carlo simulations on a cylinder model [23] in which none or few co-ions are present and the counterions hard core is small compared to the DNA radius, i.e., $\sigma/a'_0 \sim 0.1$. In addition, Monte Carlo simulations were performed to investigate the effects of dielectric saturation of water near DNA, using a more detailed molecular structure of the polyion, a structure based on experimental coordinates [24]. The PB equation does not include the ion-ion correlations due to the finite size of the ions, as opposed to the simulations in which these correlations are considered.

The results of the simulations show that the radial counterion distribution obtained by the PB equation is in qualitative agreement with the simulations. If a smaller value of the dielectric constant for the solvent close the polyion is introduced in the PB equation, a better agreement can be obtained (using the bulk dielectric constant of water in the PB equation, counterion concentration at close distances is underestimated by approximately 18% [24] with respect to the results of the simulations). In our paper, the value of this dielectric constant is consistent with measurements performed in highly concentrated ionic solutions [32,33] and our calculations give reasonable values of other experimental parameters that are well known.

As shown in other studies [27–29], counterions can be described by the PB equation. The counterion distribution from the PB equation gives a high counterion concentration near the cylinder surface, a fact consistent with Manning's theory of counterion condensation [25,26]. Some authors have shown that a lower dielectric constant for the solvent near the DNA polyion enhances the counterion condensation [24,30]. A lower dielectric constant near the DNA polyion is consistent with the fact that in highly concentrated ionic solutions the dielectric constant of water is lower than for pure water [31–33]. Hence, in solving the PB equation, we have used two dielectric constants, one corresponding to the bulk solvent, and the other to the solvent close to the cylindrical surface.

For an infinite charged cylinder, which is surrounded by counterions of one type, the PB equation is

$$\nabla^2 \tilde{\phi}(r) = \frac{1}{r} \frac{\partial}{\partial r} \left(r \frac{\partial \tilde{\phi}(r)}{\partial r} \right) = \begin{cases} -\frac{4\pi}{\tilde{\epsilon}} \tilde{\rho}(r) & \text{for } a_0 \leq r \leq a \\ -\frac{4\pi}{\epsilon} \tilde{\rho}(r) & \text{for } a < r \leq R, \end{cases} \quad (4.1a)$$

where r is the radial distance to the axis; the two dielectric constants are $\tilde{\epsilon}$ for the solvent close to the cylindrical surface, within $a_0 \leq r \leq a$, and ϵ for the bulk solvent, in $a < r \leq R$. A picture of the cylinder model is displayed in Fig. 4. The charge density $\tilde{\rho}(r)$ is determined by the statistical Boltzmann factor,

$$\tilde{\rho}(r) = qn_0 e^{-q\tilde{\phi}(r)/k_B T}, \quad (4.1b)$$

where q is the charge of the counterions, $q\tilde{\phi}(r)$ is the average potential energy of a counterion in the solution or the potential of mean force (PMF) of the counterion at a distance r from the cylinder (polyion), qn_0 is the charge density at a distance where $\tilde{\phi}(r) = 0$, and T is the absolute temperature.

In a first approximation, because of the negative sign in the exponent of the exponential function, the occurrence of ions with the same sign of charge as the cylinder (co-ions) is neglected; therefore we assume that the only ions in solution are the counterions. In addition, the counterion potential energies are relevant to the extent they are comparable to $k_B T$; at room temperature (25 °C), $k_B T \approx 0.026$ eV.

The general solution of Eqs. (4.1a) and (4.1b) is

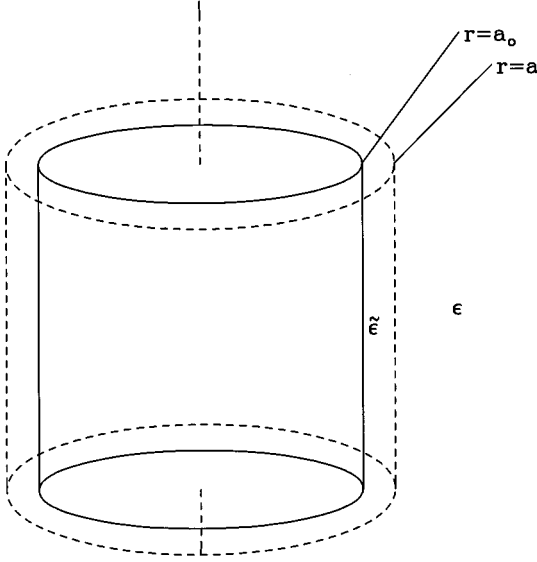


FIG. 4. Uniformly charged cylinder of infinite length in solution. Solid lines represent the impenetrable cylinder of radius a_0 , where $a_0 = a'_0 + \sigma$. In this equation, a'_0 is the radial distance of the charges to the axis of the double helix and σ is the minimum distance of approach of a counterion to a helix charge. The solution is on the outside of the cylinder. The dielectric constant for the solvent is $\tilde{\epsilon}$ at close distances, $a_0 \leq r \leq a$, and ϵ at large distances, $a < r \leq R$. The length parameter R , used in solving the Poisson-Boltzmann equation, is not shown.

$$\tilde{\phi}(r) = \begin{cases} \frac{k_B T}{q} \ln \left[\frac{\kappa^2 r^2}{2(\tilde{\epsilon}/\epsilon)\tilde{\beta}_0} \sinh^2[\tilde{\beta}_0 \ln(A_0 r)] \right] & \text{for } a_0 \leq r \leq a \\ \frac{k_B T}{q} \ln \left[\frac{\kappa^2 r^2}{2\tilde{\beta}^2} \sinh^2[\tilde{\beta} \ln(Ar)] \right] & \text{for } a < r \leq R, \end{cases} \quad (4.2)$$

where $\kappa^2 = 4\pi q^2 n_0 / \epsilon k_B T$. The parameter $1/\kappa$ is related to the thickness of the counterion diffuse cloud.

The four constants $\tilde{\beta}$, $\tilde{\beta}_0$, A , and A_0 in Eq. (4.2) are determined by requiring the continuity at $r=a$ of the potential $\tilde{\phi}(r)$ and the associated electric field, and two additional conditions: (i) the space integral of the charge of the counterions in solution is equal in magnitude and opposite in sign to the surface charge on the cylinder; (ii) the electric field vanishes at a radius R within which the counterions are confined.

Condition (i) assures the electrical neutrality of the solution and condition (ii) is used for convenience. From condition (i), we get

$$\lambda = - \int_{a_0}^R \tilde{\rho}(r') 2\pi r' dr',$$

where λ is the linear charge density of the cylinder and a_0 is the radius of the cylinder or the distance of closest approach of a counterion to the cylinder axis. Using Eq. (4.1a) in the last equation, we get

$$\lambda = \frac{\tilde{\epsilon}}{2} \left(r' \frac{\partial \tilde{\phi}(r')}{\partial r'} \right)_{r'=a} - \frac{\tilde{\epsilon}}{2} \left(r' \frac{\partial \tilde{\phi}(r')}{\partial r'} \right)_{r'=a_0} + \frac{\epsilon}{2} \left(r' \frac{\partial \tilde{\phi}(r')}{\partial r'} \right)_{r'=R} - \frac{\epsilon}{2} \left(r' \frac{\partial \tilde{\phi}(r')}{\partial r'} \right)_{r'=a},$$

or

$$\lambda = - \frac{\tilde{\epsilon} a_0}{2} \left(\frac{\partial \tilde{\phi}(r')}{\partial r'} \right)_{r'=a_0}. \quad (4.3)$$

Using condition (ii) and the continuity of the electric field at $r=a$:

$$\tilde{\epsilon} \left[r' \frac{\partial \tilde{\phi}(r')}{\partial r'} \right]_{r'=a-\delta} = \epsilon \left[r' \frac{\partial \tilde{\phi}(r')}{\partial r'} \right]_{r'=a+\delta} \quad (\lim \delta \rightarrow 0), \quad (4.4a)$$

or, using Eq. (4.2),

$$\tilde{\epsilon} \{ 1 + \tilde{\beta}_0 \coth[\tilde{\beta}_0 \ln(A_0 a)] \} = \epsilon \{ 1 + \tilde{\beta} \coth[\tilde{\beta} \ln(Aa)] \}. \quad (4.4b)$$

The continuity of the potential is

$$[\tilde{\phi}(r')]_{r'=a-\delta} = [\tilde{\phi}(r')]_{r'=a+\delta} \quad (\lim \delta \rightarrow 0). \quad (4.5)$$

We introduce the following parameter, which turns out to be important in Manning's theory:

$$\xi = - \frac{q\lambda}{\epsilon k_B T}. \quad (4.6)$$

ξ is a positive number because q and λ have opposite signs. The linear charge density λ is determined by Eq. (3.6) of the previous section.

From Eqs. (4.2), (4.3), and (4.6), we find that

$$\xi = (\tilde{\epsilon}/\epsilon) \{ 1 + \tilde{\beta}_0 \coth[\tilde{\beta}_0 \ln(A_0 a_0)] \}, \quad (4.7)$$

which can be written as

$$\xi = (\tilde{\epsilon}/\epsilon) \left[1 + \frac{[(\tilde{\epsilon}/\epsilon)\xi_f - 1] \tilde{\beta}_0 \coth[\tilde{\beta}_0 \ln(a_0/a)] + \tilde{\beta}_0^2}{[(\tilde{\epsilon}/\epsilon)\xi_f - 1] + \tilde{\beta}_0 \coth[\tilde{\beta}_0 \ln(a_0/a)]} \right], \quad (4.8a)$$

where

$$\tilde{\beta}_0^2 = 1 + (\tilde{\epsilon}/\epsilon) \{ [(\tilde{\epsilon}/\epsilon) - 1] \xi_f^2 - (1 - \tilde{\beta}^2) \} \quad (4.8b)$$

and

$$\xi_f = \frac{1 - \tilde{\beta}^2}{1 + \tilde{\beta} \coth[\tilde{\beta} \ln(R/a)]}. \quad (4.8c)$$

From known values of the parameters ξ , ϵ , $\tilde{\epsilon}$, a_0 , a , and R , the last three equations can be solved for $\tilde{\beta}$, $\tilde{\beta}_0$, and ξ_f . The parameter ξ_f is proportional to the effective linear charge density at the radius $r=a$, after the counterions near the cylinder have partially neutralized the charged surface. In

expressing $\bar{\beta}_0^2$ in Eq. (4.8b), we have used Eqs. (4.2), (4.4b), and (4.5). The expression for ξ_f in Eq. (4.8c) resulted from combining

$$\xi_f = \{1 + \bar{\beta} \coth[\bar{\beta} \ln(Aa)]\} \quad (4.9a)$$

and

$$0 = 1 + \bar{\beta} \coth[\bar{\beta} \ln(AR)], \quad (4.9b)$$

which results from condition (ii), given above. To obtain values for ξ with physical meaning, it can be seen, using Eqs. (4.8a)–(4.8c), that the values of $\bar{\beta}$ which give a value of ξ within the range $0 < \xi < \infty$ are either real, $1 \geq \bar{\beta} \geq 0$, or purely imaginary, $0 < \bar{\beta} < i\bar{\beta}_\infty$, where $\bar{\beta}_\infty$ is a certain real value. (The parameters ξ and ξ_f are real quantities because they are proportional to a linear charge density; therefore $\bar{\beta}$ and $\bar{\beta}_0$ must be either real or purely imaginary constants.) To accurately solve Eqs. (4.8a)–(4.8c), values of $\bar{\beta}$ within the mentioned range are substituted, until the desired value of ξ is obtained. [For our purposes, the values of $\bar{\beta}$ and $\bar{\beta}_0$ are designated as positive, and either real or imaginary, because the formulas are invariant after a change in sign. In using imaginary values, $\coth(is) = -i \cot(s)$ where s is the argument.]

To analyze the counterion distribution, we calculate the following functions:

$$\bar{p}(r)dr = \frac{\bar{\rho}(r)2\pi r}{\int_{a_0}^R \bar{\rho}(r')2\pi r' dr'} dr, \quad (4.10a)$$

$$\bar{p}(r)dr = \begin{cases} \left[\frac{(\bar{\epsilon}/\epsilon)(\bar{\beta}_0^2/\xi)}{r \sinh^2[\bar{\beta}_0 \ln(A_0 r)]} \right] dr & \text{for } a_0 \leq r \leq a \\ \left[\frac{\bar{\beta}^2/\xi}{r \sinh^2[\bar{\beta} \ln(AR)]} \right] dr & \text{for } a < r \leq R, \end{cases} \quad (4.10b)$$

and

$$\bar{\Theta}(r) = \int_{a_0}^r \bar{p}(r') dr' = \frac{\int_{a_0}^r \bar{\rho}(r')2\pi r' dr'}{\int_{a_0}^R \bar{\rho}(r')2\pi r' dr'}, \quad (4.11a)$$

$$\bar{\Theta}(r) = \begin{cases} 1 - \frac{(\bar{\epsilon}/\epsilon)}{\xi} \{1 + \bar{\beta}_0 \coth[\bar{\beta}_0 \ln(A_0 r)]\} & \text{for } a_0 \leq r \leq a \\ 1 - \frac{1}{\xi} \{1 + \bar{\beta} \coth[\bar{\beta} \ln(AR)]\} & \text{for } a < r \leq R. \end{cases} \quad (4.11b)$$

In the last formulas, A and A_0 are determined by solving Eqs. (4.7) and (4.9a). Equations (4.10a) and (4.10b) give the probability that a counterion is found between the distances r and $r+dr$ from the axis. Equations (4.11a) and (4.11b) represent the probability of having a counterion within a distance r , or the fraction of the total charge in solution that lies between the radius a_0 and r . When ξ is large, most of the

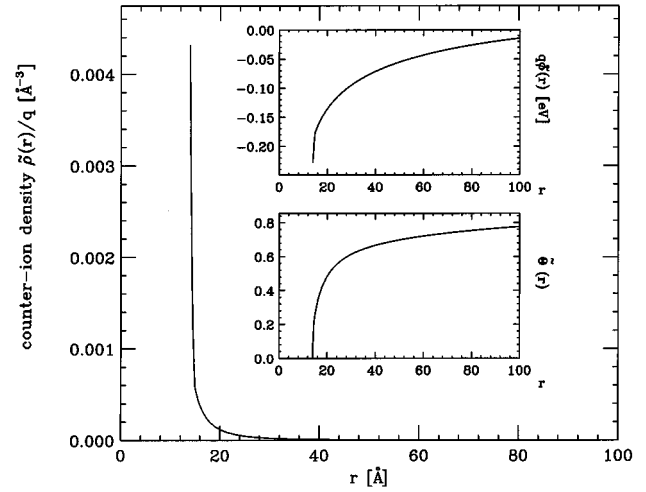


FIG. 5. The counterion density given in Eq. (4.1b) is shown. In the upper inset is the potential energy of a unit charge counterion, $q = |e|$, near the charged cylinder, from Eq. (4.2). In the lower inset is the fraction of the total counterion charge that is within a radius r , plotted from Eq. (4.11b). At $r=R$, $\bar{\Theta}(r)$ is unity (not shown). Near the cylinder radius a large fraction of charge is accumulated. The values of the parameters, defined within the text, are $\xi = 4.43$ [$h(\psi_Y) = 3.21$ Å, $\bar{\beta} = i0.6844$], $\epsilon = 78.85$, $\bar{\epsilon} = 20$, $a_0 = 14$ Å, $a = 15$ Å, $R = 403.5$ Å, $n_0 = 0.001M$, and $T = 298.15$ K.

counterions remain close to the surface. In Eq. (4.11b), the quantity in the right-hand side enclosed in braces for $a < r \leq R$ decreases when r increases. This quantity decreases sharply when r is still close to a and slowly when r increases more towards $r=R$, where it vanishes. The large concentration of counterions near the cylinder surface is consistent with Manning's theory of counterion condensation because the quantity in braces in Eq. (4.11b) is close to 1 at a somewhat arbitrary radius which is close to the surface. In Manning's theory, the fraction of condensed counterions approaches the limit $1 - 1/\xi$ [25,26].

The charge density $\bar{\rho}(r)$ in Eq. (4.1b) is not determined completely unless the constant n_0 is known. In our calculation, the concentration n_0 , which is fixed, is defined in terms of the volume of solution per counterion. With this definition we have a lower limit for the bulk concentration. The expression for n_0 is

$$n_0 = \frac{1}{(d_{pp}/2)\pi(R^2 - a_0^2)}, \quad (4.12)$$

where d_{pp} is the distance between two consecutive charges on the same chain of the helix, as described in Sec. III.

Because of Eq. (4.1b), the presence of the charged cylinder causes the charge density of counterions, $\bar{\rho}(r)$, to be sharply peaked at the cylinder surface, as shown in Fig. 5. The local counterion charge density at the surface varies quite rapidly. The high concentration of counterions is also apparent in an inset of Fig. 5, where Eq. (4.11b) is plotted. This equation gives the fraction of counterions around the cylinder within a radius r .

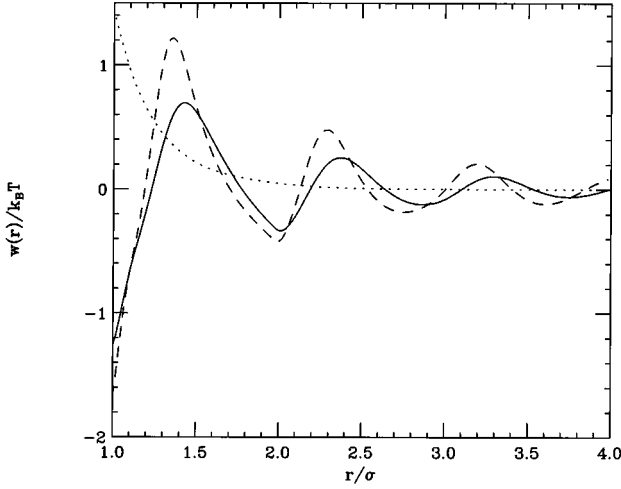


FIG. 6. The PMF at several counterion concentrations during coiling from Eqs. (2.4a)–(2.4c) and (4.14). The parameters are given in Table III, section (a), item 1, where $\tilde{\epsilon}=15$. Symbols are explained in text. A unit charge is assumed for each of the charges on the helix and the counterions, i.e., $q' = -|e|$ and $q = |e|$. The curves correspond to various coiled conformations: $\psi_Y = 0^\circ$, $c = 0.84M$, $\xi = 2.19$, dotted line; $\psi_Y = 36.0^\circ$, $c = 7.57M$, $\xi = 4.23$, solid line; $\psi_Y = 36.5^\circ$, $c = 8.47M$, $\xi = 4.39$, dashed line. c is calculated from Eq. (4.15b).

The charges on the polyion are restricted to the surface of the cylinder; therefore, we determine the local concentration using $\tilde{\rho}(a_0)$ at the surface, namely,

$$n = \frac{\tilde{\rho}(a_0)}{q}, \quad (4.13)$$

where q is the charge of a counterion; Eqs. (4.1b), (4.12), and (4.2) are used. The local ionic concentration, shown in Eq. (4.13), is substituted in the PMF, given in Eqs. (2.4a)–(2.4d). The inverse DH screening length associated with the counterions near the double helix is

$$k = \left(\frac{4\pi n q'}{\tilde{\epsilon} k_B T} \right)^{1/2}, \quad (4.14)$$

which is used instead of Eq. (2.4d), and n is given by Eq. (4.13). [A charge on the double helix denoted by q' replaces q_1 in Eq. (2.4c).] The interactions between charges on the helix are calculated by the PMF, which is illustrated in Fig. 6. This calculation is required in order to obtain the difference in the free energy between the two conformations, $\Delta W(Y, X)$, given in Eqs. (3.5a)–(3.5d).

If n and n_0 are given in number of counterions per \AA^3 , the molar concentrations (M) are

$$c_0 = \frac{n_0}{6.022 \times 10^{-4}}, \quad (4.15a)$$

$$c = \frac{n}{6.022 \times 10^{-4}}, \quad (4.15b)$$

TABLE II. The parameters of the double helix model which are based on *A*-DNA and *B*-DNA experimental parameters of Table I. It is seen that the two models only differ in the value of the distance between consecutive charges on the same chain, d_{pp} .

Type	a'_0 (\AA)	\bar{d}_{pp} (\AA)	$\bar{\psi}_0$ (deg)	\bar{h}_0^a (\AA)	d_{pp} (\AA)
<i>A</i> model	9	18.2	170	3.12	5.6
<i>B</i> model	9	18.2	170	3.12	6.5

^aCalculated from Eq. (3.2) in text.

where n_0 and n are given by Eqs. (4.12) and (4.13), respectively.

V. RESULTS ON THE FREE ENERGY OF COILING

In this section, we discuss the results of the calculations on the change in the free energy between the coiled and uncoiled conformations, $\Delta W(Y, X)$. The parameters for two double helix models are shown in Table II. The *A* model and the *B* model, which we use for the calculations, are based on the experimental values of Table I and they correspond to *A*-DNA and *B*-DNA, respectively. The only difference between these models is the value of d_{pp} , the distance between two consecutive charges on the same chain. For the calculations, the change in the value of d_{pp} is what seems to be essential. The results of the calculations are shown in Figs. 6–13 and Tables III–VI. The values of the parameters shown in these tables are both experimental and calculated; the calculated ones are noted with an asterisk. In Figs. 7–13, $\Delta W(Y, X)$, which is calculated from Eqs. (3.5a)–(3.5d) of Sec. III, is shown as a function of the coiling angle ψ_Y of conformation *Y*; the corresponding values of the molar local concentration of counterions, calculated from Eq. (4.15b), are also shown. The calculations are based on the pair potential of mean force given in Eqs. (2.4a)–(2.4c) of Sec. II and Eq. (4.14) of Sec. IV; we assumed that a charge on the helix and a counterion is a unit charge; the PMF is illustrated in Fig. 6. In Eqs. (2.4c) and (4.14), the dielectric constant that enters in the PMF, $\tilde{\epsilon}$ is equal to the dielectric constant for the solvent near the cylinder which is used in Sec. IV; this is so because the charges on the helix are immersed in this solvent. Tables III–VI are divided into sections, which are labeled with a letter, and within each table section we give various examples, which are labeled with a number (in the first column). Each of the seven table sections is shown in each of Figs. 7–13. In Tables III–VI, the experimental parameters that are fixed for the examples of the table section are shown in the heading. In the first six columns, the calculated parameters which minimize the value of the change in the free energy, $\Delta W(Y, X)$, are noted with an asterisk. In the last two columns of Tables IV–VI, we give two experimental parameters that change in each example. In the following paragraphs, we explain the results for each table section.

(a) We use the parameters of the *B* model, which is given in Table II, appropriate for aqueous solutions. As seen in Fig. 7, decreasing the dielectric constant for the solvent near the double helix, $\tilde{\epsilon}$, causes the change in the free energy, $\Delta W(Y, X)$, to decrease and the position of the minimum to approach zero at a certain critical value of $\tilde{\epsilon}$. The value of 20 for $\tilde{\epsilon}$ is chosen in the following water solution examples

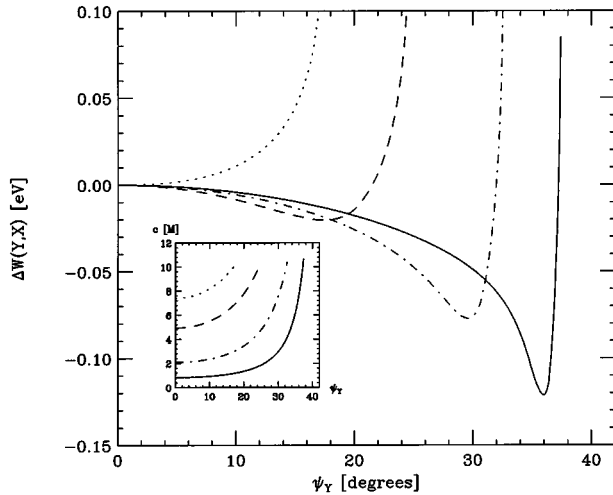


FIG. 7. The dielectric constant for the solvent near to the helix, $\bar{\epsilon}$, is varied. The change in the free energy, $\Delta W(Y,X)$, between two conformations Y (coiled) and X (uncoiled) is shown, calculated from Eq. (3.5a), as a function of the angle ψ_Y of Y . Inset: local counterion concentration c from Eq. (4.15b). The double helix parameters are from the B model of Table II. Each charge on the helix is a unit charge. The parameters of these examples are given in section (a) of Table III. The following numbers refer to the first column of Table III: 1 (solid line), 2 (dot-dashed line), 3 (dashed line), and 4 (dotted line). The value of $\bar{\epsilon}$ decreases in the order 1-2-3-4.

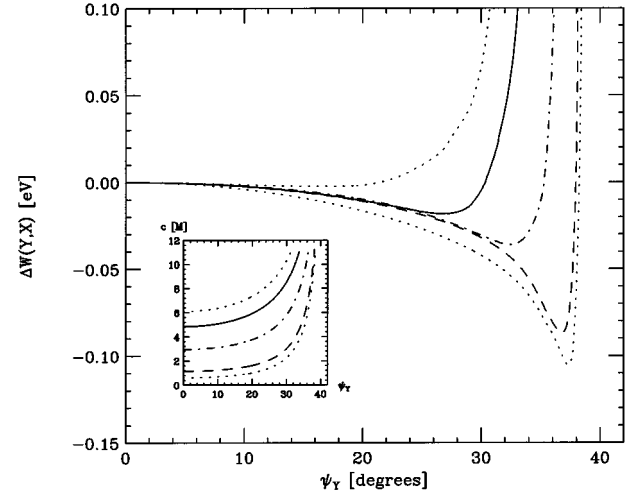


FIG. 9. The bulk concentration c is varied, using $\sigma=5.85 \text{ \AA}$. The change in the free energy, $\Delta W(Y,X)$, between two conformations Y (coiled) and X (uncoiled) is shown, calculated from Eq. (3.5a), as a function of the angle ψ_Y of Y . Inset: local counterion concentration c from Eq. (4.15b). The double helix parameters are obtained from the B model of Table II. Each charge on the helix is a unit charge. The parameters of these examples are given in section (c) of Table IV. The following numbers refer to the first column of Table IV: 1 (dotted line), 2 (dashed line), 3 (dot-dashed line), 4 (solid line), and 5 (upper dotted line). The value of c increases in the order 1-2-3-4-5.

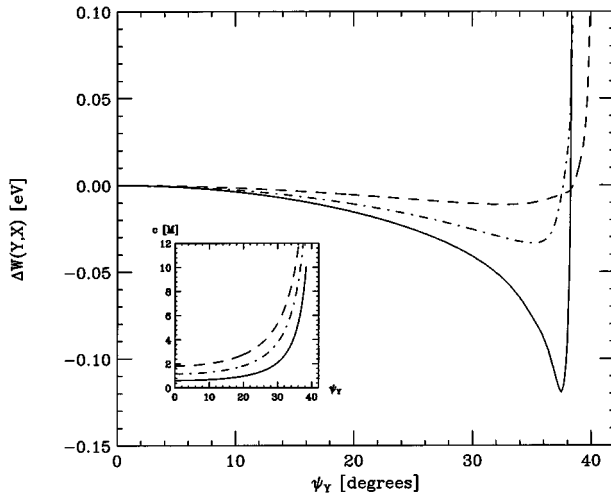


FIG. 8. The minimum distance of approach of a counterion to a charge on the helix, σ is varied. The change in the free energy, $\Delta W(Y,X)$, between two conformations Y (coiled) and X (uncoiled) is shown, calculated from Eq. (3.5a), as a function of the angle ψ_Y of Y . Inset: local counterion concentration c from Eq. (4.15b). The double helix parameters are obtained from the B model of Table II. Each charge on the helix is a unit charge. The parameters of these examples are given in section (b) of Table III. The following numbers refer to the first column of Table III: 1 (solid line), 2 (dot-dashed line), and 3 (dashed line). The value of σ decreases in the order 1-2-3.

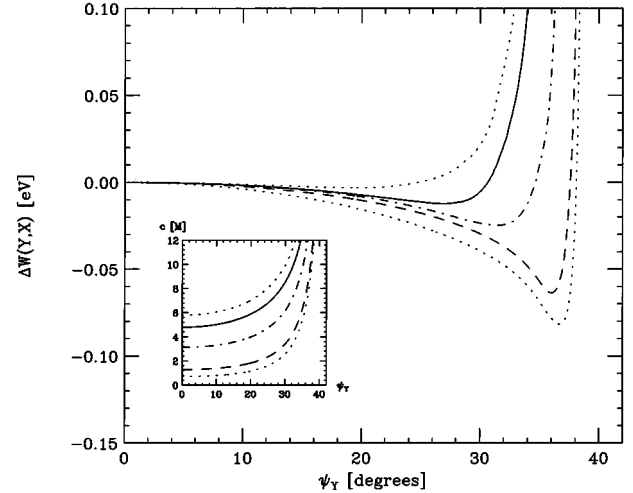


FIG. 10. The bulk concentration c is varied, using $\sigma=5.65 \text{ \AA}$. The change in the free energy, $\Delta W(Y,X)$, between two conformations Y (coiled) and X (uncoiled) is shown, calculated from Eq. (3.5a), as a function of the angle ψ_Y of Y . Inset: local counterion concentration c from Eq. (4.15b). The double helix parameters are obtained from the B model of Table II. Each charge on the helix is a unit charge. The parameters of these examples are given in section (d) of Table IV. The following numbers refer to the first column of Table IV: 1 (dotted line), 2 (dashed line), 3 (dot-dashed line), 4 (solid line), and 5 (upper dotted line). The value of c increases in the order 1-2-3-4-5.

because this value is consistent with measurements in concentrated ionic solutions [32,33] and it yields reasonable values for the other parameters. The parameter c^* is calculated from Eq. (4.15b). Figure 6 illustrates the PMF, given in Eqs. (2.4a)–(2.4c) and (4.14), that was used in the calculation. The PMF is not a monotonic function of r and this feature might produce kinks in $\Delta W(Y,X)$, as seen in Figs. 11 and 12.

(b) This shows a change in the radius of the counterion, which changes the counterion minimum distance of approach (hard core) to the center of a charge on the double helix. As seen in Fig. 8, after decreasing the radius of the counterion the change in the free energy is smaller. The calculations suggest that the *B*-DNA might be unstable for small radii of the counterion. However, counterion hydrated radii are not too small, about 5 Å [32,33], if we include both the diameter of a water molecule and the ionic radius of the counterion. Because of the high concentration of counterions near the double helix, the Coulomb interaction is screened and the nonmonotonic hard-core correlation effects become important, as shown in Fig. 6. Even though the sum of Eq. (3.5a) can be performed easily to include the first 200 charges, the nearest charges in the same chain contribute significantly to the change in the free energy. These results are consistent with the experimental finding that with counterions of large hydrated radii (small ionic radii), DNA is more stable. For DNA in *aqueous* solution, the temperature of melting is higher in Li^+ compared to Na^+ [40], and in Na^+ compared to K^+ [41]. The hydrated radius of the counterion decreases in the order $\text{Li}^+ > \text{Na}^+ > \text{K}^+$.

(c) and (d) These illustrate the change in the bulk concentration c_0 from Eq. (4.15a) with a corresponding change in the dielectric constant for the solution, ϵ . The value of these parameters are obtained from Refs. [32] and [33], where the hydrated radii of three counterions in aqueous solution and the static dielectric constant were measured. (The radii decrease in the order $\text{Li}^+ > \text{Rb}^+ > \text{Cs}^+$.) Table sections (c) and (d) correspond to Li^+ and Cs^+ , respectively. The measured hydrated radii for Li^+ , Cs^+ , and Cl^- are 2.6, 2.4, and 3.25 Å, respectively. The hard core σ is obtained by adding the radii of a positive and a negative ion, resulting in 5.85 and 5.65 Å. (We use the hydrated radius of Cl^- for the hydrated radius of the phosphate groups on the double helix.) As seen in Figs. 9 and 10, for (c) and (d), respectively, the double helix is less coiled [the value of ψ_Y at the minimum of $\Delta W(Y,X)$, ψ_Y^* , is reduced] when the bulk concentration is increased, which also causes a reduction of $\Delta W(Y,X)$ at the minimum. The calculations suggest that there is an uncoiling transition at sufficiently high concentrations. This uncoiling transition is different from the uncoiling transition that is observed experimentally in DNA for sufficient dilution. In our model, the local counterion concentration is calculated by solving the PB equation for an infinite cylinder. Consequently, the counterion concentration near the cylinder does not decrease substantially, even at extremely low bulk concentrations, and hence the double helix remains coiled. We have performed calculations, to be published, on the ionic concentration near a polyion of finite length. These calculations show that if the DH screening length associated with the bulk ionic concentration is comparable to or larger than the length of the polyion (or some other characteristic

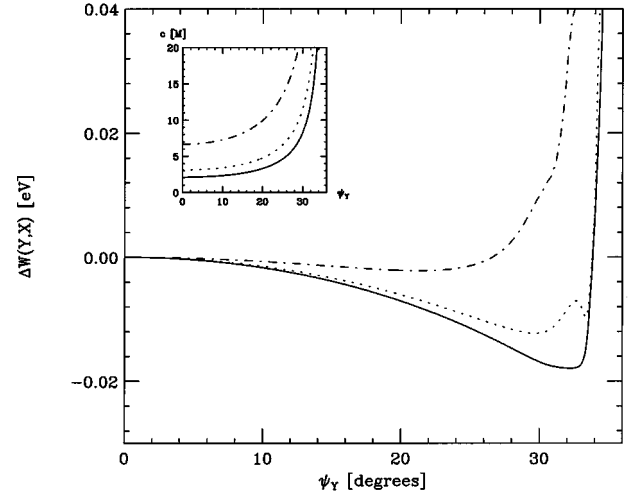


FIG. 11. The bulk dielectric constant ϵ is varied, using $\sigma = 3.79$ Å. The change in the free energy, $\Delta W(Y,X)$, between two conformations Y (coiled) and X (uncoiled) is shown, calculated from Eq. (3.5a), as a function of the angle ψ_Y of Y . Inset: local counterion concentration c from Eq. (4.15b). The double helix parameters are obtained from the *A* model of Table II. Each charge on the helix is a unit charge. The parameters of these examples are given in section (e) of Table V. The following numbers refer to the first column of Table V: 1 (solid line), 2 (dotted line), and 3 (dot-dashed line). The value of ϵ decreases in the order 1-2-3.

length scale, such as the radius of curvature), the ionic concentration at close distances decreases. A decrease of the local counterion concentration causes the helix to uncoil.

(e) and (f) These show a change of the dielectric constant

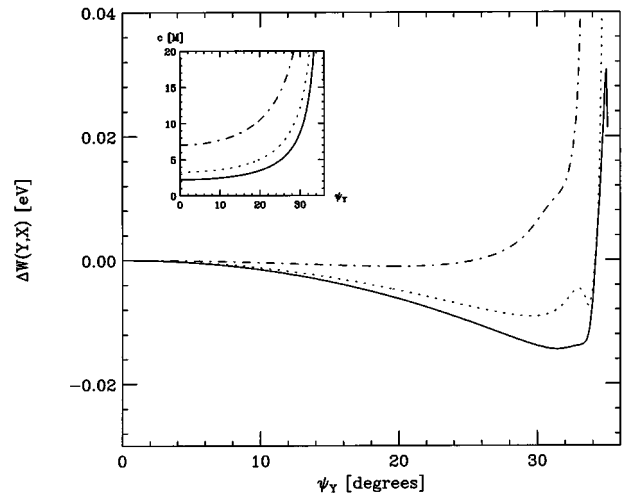


FIG. 12. The bulk dielectric constant ϵ is varied, using $\sigma = 3.45$ Å. The change in the free energy, $\Delta W(Y,X)$, between two conformations Y (coiled) and X (uncoiled) is shown, calculated from Eq. (3.5a), as a function of the angle ψ_Y of Y . Inset: local counterion concentration c from Eq. (4.15b). The double helix parameters are obtained from the *A* model of Table II. Each charge on the helix is a unit charge. The parameters of these examples are given in section (f) of Table V. The following numbers refer to the first column of Table V: 1 (solid line), 2 (dotted line), and 3 (dot-dashed line). The value of ϵ decreases in the order 1-2-3.

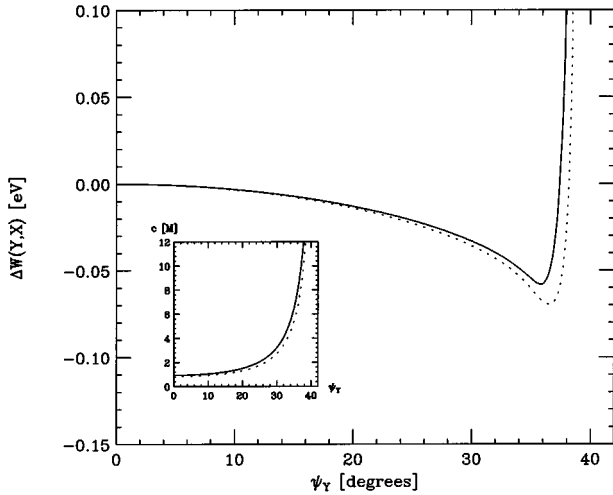


FIG. 13. The temperature is varied. The change in the free energy, $\Delta W(Y,X)$, between two conformations Y (coiled) and X (uncoiled) is shown, calculated from Eq. (3.5a), as a function of the angle ψ_Y of Y . Inset: local counterion concentration c from Eq. (4.15b). The double helix parameters are obtained from the B model of Table II. Each charge on the helix is a unit charge. The parameters of these examples are given in section (g) of Table VI. The following numbers refer to the first column of Table VI: 1 (solid line) and 2 (dotted line). The temperature T increases in the order 1-2.

for the bulk solvent ϵ . The bulk counterion concentration is low in these examples; thus we use the dielectric constant for the pure solvent. A decrease in the dielectric constant for the solvent is achieved by mixing an alcohol, such as methanol or ethanol, with the water [42]. At $T = 25^\circ\text{C}$, the values of the

dielectric constants for the pure solvents are [43] $\epsilon_w = 78.85$, $\epsilon_m = 32.63$, and $\epsilon_e = 24.3$, for water, methanol, and ethanol, respectively. The examples in Table V are calculated using the static dielectric constant of a mixture of water and ethanol, which is obtained from measurements [42]. In addition, it is found from experiments of DNA in solutions with a high content of ethanol that DNA is in the A conformation [44], i.e., A -DNA. Therefore the parameters of the A model in Table II are used in these examples. As seen from the calculations in Fig. 8 and table section (b), the B model becomes unstable for small counterion radii. In experiments, the high content of ethanol might prevent the hydration of the counterion. In a solution with small counterions, the A model is a more stable conformation; this is because consecutive phosphate groups on the same chain are closer. In our calculations, we have chosen Cs^+ and K^+ as the two counterions. The ionic radii can be obtained [43] and are found to be 2.12, 1.67, and 1.33 Å, for P (for a phosphate group), Cs, and K, respectively. The hard core σ is obtained by adding phosphate and counterion ionic radii. In these calculations, we have assumed there is no hydration; therefore there is only one value of the dielectric constant for the solvent. The values of 37.18 and 27.99 correspond to mixtures of ethanol and water where the mole fraction of water is 0.5 and 0.2, respectively [42]. As seen in Figs. 11 and 12, on decreasing the dielectric constant and the counterion radii, $\Delta W(Y,X)$ at the minimum increases. The curves in these figures have kinks, showing less coiling or more coiling, depending on the values of the parameters. Considering that the double helix uncoils before denaturation takes place, our results are consistent with measurements of DNA in ethanol and methanol solutions. It is well known that methanol and ethanol, or mixtures of these solvents and water, denature DNA [45,46], and that the denaturation temperature is lower

TABLE III. The dependence of the free energy change on the dielectric constant for the solvent near the double helix and on the counterion hard-core radius. The change in the free energy $\Delta W(Y,X)$ is calculated from Eqs. (3.5a)–(3.5d). The coiled conformation is Y and the uncoiled conformation is X . The coiling angle is ψ_Y . In each section there are experimental and calculated parameters. The calculated parameters are denoted with an asterisk. In each section, several examples are shown. The experimental parameters in the section heading remain fixed for the examples within the section.

ΔW^* (eV)	ψ_Y^* (deg)	h^* (Å)	c^* (M)	ξ^*	$\bar{\beta}^*$	$\bar{\epsilon}$	σ (Å)	a_0 (Å)
(a)								
$T = 298.15\text{ K}$ $\epsilon = 78.85$ $c_0 = 0.001\text{ M}$ ($R = 403.6\text{ Å}$) ^a								
$\sigma = 6\text{ Å}$ $a_0 = 15\text{ Å}$ $a = 16\text{ Å}$								
1	-0.121	36.0	3.36	7.57	4.23	$i0.6887$	15	
2	-0.077	29.6	4.59	7.21	3.10	$i0.6493$	8	
3	-0.020	17.4	5.90	6.91	2.41	$i0.6005$	5	
4	~ 0	0.3	6.50	7.40	2.19	$i0.5708$	4	
5	~ 0	~ 0	6.50	9.34	2.19	$i0.5554$	3.5	
(b)								
$T = 298.15\text{ K}$ $\epsilon = 78.85$ $c_0 = 0.001\text{ M}$ ($R = 403.6\text{ Å}$) ^a								
$\bar{\epsilon} = 20$ $a = 16\text{ Å}$								
1	-0.119	37.5	2.96	7.60	4.80	$i0.7005$	6	15
2	-0.033	35.1	3.58	7.32	3.98	$i0.6584$	5	14
3	-0.011	32.8	4.05	7.15	3.51	$i0.6139$	4	13

^a R is used in Eq. (4.12) in text.

TABLE IV. As Table III, showing the dependence of the free energy change on the bulk concentration of the solution.

	ΔW^* (eV)	ψ_Y^* (deg)	h^* (Å)	$c^*(M)$	ξ^*	$\bar{\beta}^*$	$c_0(M)$	ϵ
(c)								
$T=298.15 \text{ K} \quad \tilde{\epsilon}=20$								
$\sigma=5.85 \text{ Å} \quad a_0=14.85 \text{ Å} \quad a=16 \text{ Å}$								
1	-0.106	37.3	3.02	7.79	4.71	$i0.4561$	10^{-5} (4032.8) ^a	78.85
2	-0.087	36.8	3.16	7.85	4.50	$i1.5311$	0.1 (43.0)	78.85
3	-0.036	32.4	4.13	6.93	4.23	$i3.4609$	1.09 (19.2)	64.2
4	-0.018	26.7	5.00	7.27	4.62	$i5.4189$	2.65 (16.8)	48.6
5	-0.002	16.0	6.00	6.83	4.57	$i6.6178$	3.88 (16.2)	40.95
(d)								
$T=298.15 \text{ K} \quad \tilde{\epsilon}=20$								
$\sigma=5.65 \text{ Å} \quad a_0=14.65 \text{ Å} \quad a=16 \text{ Å}$								
1	-0.082	36.7	3.18	7.49	4.47	$i0.4523$	10^{-5} (4032.8) ^a	78.85
2	-0.064	35.9	3.39	7.27	4.20	$i1.4824$	0.1 (42.9)	78.85
3	-0.025	31.5	4.29	6.82	3.85	$i3.2375$	1.1 (19.0)	68.0
4	-0.012	26.9	4.97	7.30	3.92	$i4.7170$	2.5 (16.7)	57.6
5	-0.003	16.2	5.72	6.98	3.77	$i5.5459$	3.5 (16.2)	52.1

^a R in Å, which is used in Eq. (4.12) in text.

compared to an aqueous solution of the same ionic concentration. Experimentally, it is found that DNA in methanol solutions is more stable when the ionic radius of the counterion is larger [45,44], as opposed to what happens in pure

water. The melting temperature decreases in Na^+ as compared to Cs^+ [45], which is understood because Cs^+ has the larger ionic radius. As noted in other studies [9,12], the stability of the double stranded DNA secondary structure is not

TABLE V. As Table III, showing the dependence of the free energy change on the dielectric constant for the bulk solvent.

	ΔW^* (eV)	ψ_Y^* (deg)	h^* (Å)	$c^*(M)$	ξ^*	$\bar{\beta}^*$	ϵ	$\tilde{\epsilon}$
(e)								
$T=296.15 \text{ K} \quad c_0=0.001M \quad (R=434.7 \text{ Å})^a$								
$\sigma=3.79 \text{ Å} \quad a_0=12.79 \text{ Å}$								
1	-0.018	32.3	2.51	13.17	12.10	$i0.6999$	37.18	37.18
2	-0.012	29.7	3.18	11.01	12.70	$i0.7007$	27.99	27.99
3	-0.002	21.4	4.49	10.67	16.75	$i0.7043$	15.0	15.0
(f)								
$T=296.15 \text{ K} \quad c_0=0.001M \quad (R=434.7 \text{ Å})^a$								
$\sigma=3.45 \text{ Å} \quad a_0=12.45 \text{ Å}$								
1	-0.014	31.4	2.76	11.26	10.99	$i0.6940$	37.18	37.18
2	-0.009	29.6	3.20	11.45	12.62	$i0.6962$	27.99	27.99
3	-0.001	20.0	4.65	10.48	16.19	$i0.6995$	15.0	15.0

^a R is used in Eq. (4.12) in text.

TABLE VI. As Table III, showing the dependence of the free energy change on the temperature.

	ΔW^* (eV)	ψ_Y^* (deg)	h^* (Å)	$c^*(M)$ (g)	ξ^*	$\bar{\beta}^*$	T (K)	ϵ
				$\bar{\epsilon}=20$				
				$c_0=0.001M$				
				$(R=403.6 \text{ Å})^a$				
				$\sigma=5.5 \text{ Å}$				
				$a_0=14.5 \text{ Å}$				
				$a=16 \text{ Å}$				
1	-0.058	35.8	3.41	7.49	4.06	<i>i</i> 0.6730	273.15	88.28
2	-0.070	36.5	3.24	7.21	4.55	<i>i</i> 0.6855	323.15	70.27

^a R is used in Eq. (4.12) in text.

only due to the interstrand hydrogen bonds. The authors of these references have also mentioned that denaturing agents, such as methanol and ethanol, do not specifically break the hydrogen bonds; however, they cause instability of the DNA helix. The hydrogen bonding is important in keeping the two DNA strands together [11], shown in experiments in which the composition of G-C pairs is varied; however, this might not be relevant for the coiling.

(g) This shows a change in the temperature with a corresponding change in the dielectric constant for the bulk solvent, according to experimental measurements [43]. In these examples we consider the B model in aqueous solution. The product ϵT decreases only slightly. This small decrease causes almost no effect on the parameters that minimize the change in the free energy, as seen in Fig. 13. The equilibrium value of ψ_Y moves slightly toward higher values, implying coiling of the helix and increase in the change in the free energy, i.e., it has a higher negative value. In these examples, we have not considered a change in the value of the dielectric constant near the double helix due to an increase of the temperature. However, this temperature dependence might be an important feature to investigate. In our model, for a very high temperature (thousands of degrees), where the dielectric constant of water is close to 1, the helix uncoils because the counterion concentration near the helix decreases enough. This temperature of uncoiling is not consis-

tent with the thermal denaturation of DNA that occurs below $T=100^\circ\text{C}$. However, a decrease of the dielectric constant for the solvent close to the helix can produce an uncoiling transition at temperatures close to the experimental value, as seen above in part (a) of this discussion and the examples shown in Fig. 7 and Table III.

As a final point, we discuss briefly the calorimeter measurements of the enthalpy associated with DNA denaturation. At a temperature of $T=25^\circ\text{C}$, $k_B T \sim 0.026$ eV. The stability of the helix depends on comparing the minimum value of the free energy of coiling with $k_B T$. Once the hydrogen bonding contribution to the energy has been subtracted, the experimental energy attributed to the stacking enthalpy is 3.6 kcal per mole of phosphate group pairs [47]. The energy attributed only to the stacking could also include the coiling energy. To compare the experimental measurement to our calculations, an energy of 1.8 kcal per mole of phosphate group (one half of the above value for one charge on the helix) is approximately 0.078 eV. The coiling energy calculated in the examples is seen to be consistent with this value.

ACKNOWLEDGMENTS

We acknowledge support from the Office of Naval Research. We also appreciate the valuable comments of Angel E. García and E. W. Prohofsky.

-
- [1] W. Saenger, *Principles of Nucleic Acid Structure* (Springer-Verlag, New York, 1980), Chaps. 4–6, 9, 11, and 17.
- [2] S. Arnott, R. Chandrasekaran, and E. Selsing, in *Structure and Conformation of Nucleic Acids and Protein-Nucleic Acid Interactions*, edited by M. Sundaralingam, and S. T. Rao (University Park Press, Baltimore, 1975), p. 577.
- [3] A. G. W. Leslie, S. Arnott, R. Chandrasekaran, and R. L. Rattliff, *J. Mol. Biol.* **143**, 49 (1980).
- [4] D. M. Soumpasis, *Proc. Natl. Acad. Sci. U.S.A.* **81**, 5116 (1984).
- [5] D. M. Soumpasis, J. Wiechen, and T. M. Jovin, *J. Biomol. Struct. Dyn.* **4**, 535 (1987).
- [6] S. Arnott and D. W. L. Hukins, *Biochem. Biophys. Res. Commun.* **47**, 1504 (1972).
- [7] D. A. Marvin, M. Spencer, M. H. Wilkins, and L. D. Hamilton, *J. Mol. Biol.* **3**, 547 (1961).
- [8] S. Arnott, R. Chandrasekaran, D. W. L. Hukins, P. J. C. Smith, and L. Watts, *J. Mol. Biol.* **88**, 523 (1974).
- [9] J. M. Sturtevant, S. A. Rice, and E. P. Geiduschek, *Discuss. Faraday Soc.* **25**, 138 (1957).
- [10] P. D. Lawley, *Biochim. Biophys. Acta* **21**, 481 (1956).
- [11] W. F. Dove and N. Davison, *J. Mol. Biol.* **5**, 467 (1962).
- [12] J. Marmur, R. Rownd, and C. L. Schildkraut, in *Progress in Nucleic Acid Research*, edited by J. N. Davidson and W. E. Cohn (Academic, New York, 1963), Vol. 1, pp. 252–254 and 265.
- [13] A. L. Lehninger, *Principles of Biochemistry* (Worth, New York, 1982), Chap. 28.
- [14] D. Lang, H. Bujard, B. Wolff, and D. Russell, *J. Mol. Biol.* **23**, 163 (1967).
- [15] L. Kotin, *J. Mol. Biol.* **7**, 309 (1963).
- [16] C. Schildkraut and S. Lifson, *Biopolymers* **3**, 195 (1965).
- [17] S. A. Rice and M. Nagasawa, *Polyelectrolyte Solutions* (Academic, London, 1961).
- [18] M. Mandel, in *Encyclopedia of Polymer Science and Engineering* (Wiley, New York, 1985), Vol. 11, pp. 739–829.
- [19] L. Kotin and M. Nagasawa, *J. Chem. Phys.* **36**, 873 (1962).
- [20] W. Olivares and D. A. McQuarrie, *Biophys. J.* **15**, 143 (1975).
- [21] R. M. Fuoss, A. Katchalsky, and S. Lifson, *Proc. Natl. Acad. Sci. U.S.A.* **37**, 579 (1951).

- [22] T. Alfrey, P. Berg, and H. Morawitz, *J. Polym. Sci.* **7**, 543 (1951).
- [23] M. Le Bret and B. H. Zimm, *Biopolymers* **23**, 271 (1984).
- [24] B. Jayaram, S. Swaminathan, D. L. Beveridge, K. Sharp, and B. Honig, *Macromolecules* **23**, 3156 (1990).
- [25] G. S. Manning, *J. Chem. Phys.* **51**, 924 (1969); **51**, 3249 (1969).
- [26] G. S. Manning, *Q. Rev. Biophys.* **11**, 179 (1978); M. T. Record, C. F. Anderson, and T. M. Lohman, *ibid.* **11**, 103 (1978).
- [27] M. Fixman, *J. Chem. Phys.* **70**, 4995 (1979).
- [28] C. F. Anderson and M. T. Record, Jr., *Annu. Rev. Phys. Chem.* **33**, 191 (1982).
- [29] B. H. Zimm and M. Le Bret, *J. Biomol. Struct. Dyn.* **1**, 461 (1983).
- [30] M. O. Fenley, G. S. Manning, and W. K. Olsen, *Biopolymers* **30**, 1191 (1990).
- [31] R. A. Robinson and R. H. Stokes, *Electrolyte Solutions* (Butterworths, London, 1959), pp. 15 and 18.
- [32] Y. Wei, P. Chiang, and S. Sridhar, *J. Chem. Phys.* **96**, 4569 (1992).
- [33] Y. Wei and S. Sridhar, *J. Chem. Phys.* **92**, 923 (1990).
- [34] L. D. Landau and E. M. Lifshitz, *Statistical Physics* (Pergamon, New York, 1980), Part I, pp. 277 and 240–242.
- [35] G. J. Throop and R. J. Bearman, *J. Chem. Phys.* **42**, 2409 (1964).
- [36] W. R. Smith and D. Henderson, *Mol. Phys.* **19**, 411 (1970).
- [37] D. A. McQuarrie, *Statistical Mechanics* (Harper and Row, New York, 1976), Appendix D.
- [38] L. Verlet and J. J. Weis, *Phys. Rev. A* **5**, 939 (1972).
- [39] R. Langridge, D. A. Marvin, W. E. Seeds, and H. R. Wilson, *J. Mol. Biol.* **2**, 38 (1960).
- [40] N. I. Korolev, A. P. Vlasov, and I. A. Kuznetsov, *Biopolymers* **34**, 1275 (1994).
- [41] H. Krakauer and J. M. Sturtevant, *Biopolymers* **6**, 491 (1971), Tables II and III.
- [42] S. Mashimo, S. Kuwabara, and S. Yagihara, *J. Chem. Phys.* **90**, 3292 (1989).
- [43] *Handbook of Chemistry and Physics*, 70th ed., edited by R. C. Weast (CRC Press, Boca Raton, 1989–1990), pp. E-51, E-57, and F-187.
- [44] V. I. Ivanov, L. E. Minchenkova, A. K. Schyolkina, and A. I. Poletayev, *Biopolymers* **12**, 89 (1973).
- [45] H. Votavova, D. Kucerova, J. Felsberg, and J. Sponar, *J. Biomol. Struct. Dyn.* **4**, 477 (1986).
- [46] T. T. Herskovits, S. J. Singer, and E. P. Geiduschek, *Arch. Biochem. Biophys.* **94**, 99 (1961).
- [47] H. Klump and T. Ackermann, *Biopolymers* **10**, 513 (1971), p. 519.